euspen's 26th International Conference & Exhibition, Krakow, PL, June 2026
www.euspen.eu

Automated Geometric Segmentation of Additively Manufactured Strut-Based Lattices for Geometric Characterization: Node – based Analysis

Y. Zekalmi [1a], D. Gallardo[2], L.C. Díaz-Pérez[2], J.A. Albajez[2], J.A. Yagüe-Fabra[2]

[1] *University of Zaragoza, Zaragoza, Spain*
[2] *I3A, Universidad de Zaragoza, Zaragoza, Spain*

[1a] *yzekalmi@unizar.es*

Abstract

The metrological characterization of strut-based lattices manufactured through additive processes is a crucial step for quality assurance and bridge the gap between nominal designs and the actual fabricated geometries. Understanding this discrepancy is particularly relevant for predicting performance, since deviations in shape, surface quality, or internal structure may significantly affect the mechanical response. In this work, we present a first approach to a general automated framework for lattice evaluation through a node – based segmentation of the structure, combining digital design models with data acquired from high-resolution X-ray computed tomography (XCT) measurements. The workflow incorporates robust geometric operations to segment and analyse individual features of the lattice, ensuring scalability and reproducibility across different unit cells and fabrication routes. Comparisons between reference models and manufactured parts allow systematic quantification of deviations, highlighting the role of process-induced imperfections on lattice morphology. This initial stage lays the foundation for a methodology that offers a flexible and reliable approach for the assessment of strut-based architectures, providing valuable insights to support optimization and performance prediction in a wide range of engineering applications.

Keywords: lattice structures, additive manufacturing, x-ray computed tomography, geometric analysis

1. Introduction

Additive manufacturing (AM) enables lattice architectures that combine low mass with tailored stiffness, energy absorption, and functional performance, making them attractive for aerospace, biomedical and lightweight engineering applications [1]. However, the as-built geometry of strut-based lattices often departs from the nominal CAD definition because the process locally alters strut cross-sections, junction morphology and surface texture, which in turn changes load paths and amplifies stress concentrations. For this reason, robust geometric verification is a prerequisite for trustworthy performance prediction and for closing the design–manufacture loop.

X-ray computed tomography (XCT) is particularly suited to lattice metrology because it provides non-destructive 3D access to internal and external geometry, but it also raises the practical challenge of making CAD-XCT comparisons repeatable at scale. Recent studies have advanced traceable XCT workflows for lattice dimensional verification using calibrated artefacts [2], and have proposed experimental strategies to determine measurement uncertainty specifically for lattice geometries [3]. Hybrid approaches that combine tactile probing with XCT have been used to strengthen dimensional metrology of complex lattices [4], while holistic XCT-based evaluation strategies have been proposed to quantify strut-level geometric characteristics across the structure [5]. In parallel, dedicated geometry-processing tools have been released to extract surface and geometric descriptors from lattice data in a more automated manner [6]. These contributions confirm the maturity of XCT for lattice inspection, yet they also highlight that most reported metrics remain global or strut-averaged, which can mask highly localized defects.

At the feature scale, node morphology is increasingly recognized as critical because junction overgrowth, under-melting, and local defects strongly influence stiffness and failure initiation. Node-focused work has included non-destructive, simulation-driven studies of node defects extracted from lattice reconstructions [7], and image-based methodologies to characterize node geometry in additively manufactured lattices [8]. More recent efforts have combined XCT with surface metrology to quantify lattice surface characteristics beyond simple dimensional error [9], and have studied how strut shape affects as-built quality and mechanical response [10]. Related investigations have examined how node size impacts lattice behaviour [11] and how geometric defects propagate in lattice-filled thin-walled structures [12]. Progress on XCT accuracy/traceability for polymer AM has been done; wall-thickness/through-hole evaluation in thin hollow lattices [13], and XCT-based porosity assessment further reinforces the need for feature-consistent, traceable characterization pipelines [14].

In this paper, we address one of the remaining gaps: XCT inspection provides high amount of metrological data; however, CAD-XCT comparison is still not consistent feature-by-feature across many repeated nodes. We exploit the known CAD topology by using CAD node centres, obtained after a proper registration. Using these positions, the XCT mesh is automatically partitioned to recover the as-manufactured node locations. This nominal–real correspondence enables consistent node-wise deviation and lattice-graph deviation analyses. The final objective is to provide a robust, automated basis for quantifying manufacturing-induced geometric variability in strut-based lattices.

2. Methodology

This section outlines the workflow to compare a designed lattice (CAD) with its manufactured geometry (obtained by XCT) in a simple, repeatable way. The method has five stages: (1) align the XCT mesh to the CAD model with a rigid best-fit, so both are in the same position and orientation; (2) read the nominal lattice layout from CAD and extract the node centers (the junction points where struts meet); (3) define a small "neighborhood" around each node (a region of influence) to look for that junction in CT; (4) assign the XCT surface points to their nearest node neighborhood, creating one small XCT sub-mesh per node; and (5) compute easy node-level descriptors (such as node offset and a graph-based deviation view along strut connections) to compare CAD vs XCT, highlight spatial trends, and flag outlier nodes for inspection.

3. Proposed node segmentation workflow

This section introduces the node-seeded workflow that converts dense XCT surfaces into topology-consistent, per-node descriptors.

Fig. 1 summarizes the nominal lattice and its graph: nodes represent junction centers and edges represent strut connectivity between nodes. This graph view is later used to define node-centered search regions so that CAD–XCT comparisons are performed feature-by-feature, not only as a global distance map.

In this work, the workflow is demonstrated and validated using a simple cubic unit cell (SC). However, the procedure is fully automated and formulated independently of the unit-cell definition, allowing node-region segmentation to be applied to lattices based on arbitrary strut-based unit-cell topologies.The graph is written as $G = (V, E)$:

• V (nodes): the junction points where struts meet (black dots in Fig. 1).

• E (edges): links between pairs of nodes. In a lattice, each edge corresponds to one strut segment between two junctions.

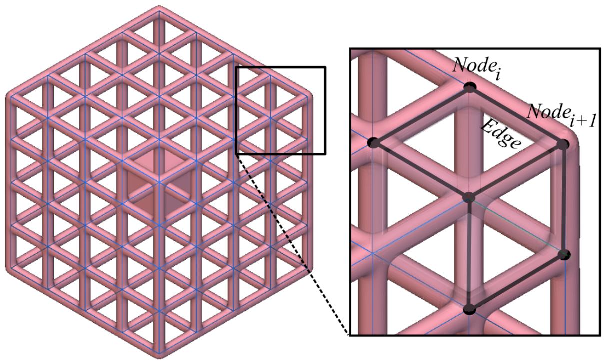

Figure 1. Lattice graph of a simple cubic unit cell. Nodes and edges.

3.1. XCT to CAD allignement and registration

Reliable CAD–XCT comparison requires aligning the XCT-derived (as-manufactured) surface with the nominal CAD lattice in a common frame. For periodic lattices, global registration can be ambiguous due to geometric symmetry, as multiple orientations may yield similar residuals. To ensure a unique and reliable initial alignment, a small reference cube is added at a known external corner of the CAD lattice. XCT mesh is then rigidly refined to the CAD using iterative closest point (ICP) algorithm with ZEISS Inspect. Fig. 2 shows the CAD–XCT deviation map and histogram: positive values mean XCT lies outside CAD, negative inside. Vertical struts (+Z) show mostly negative deviation (reduced diameter), while horizontal struts show positive deviation on top/bottom faces (expansion along Z).

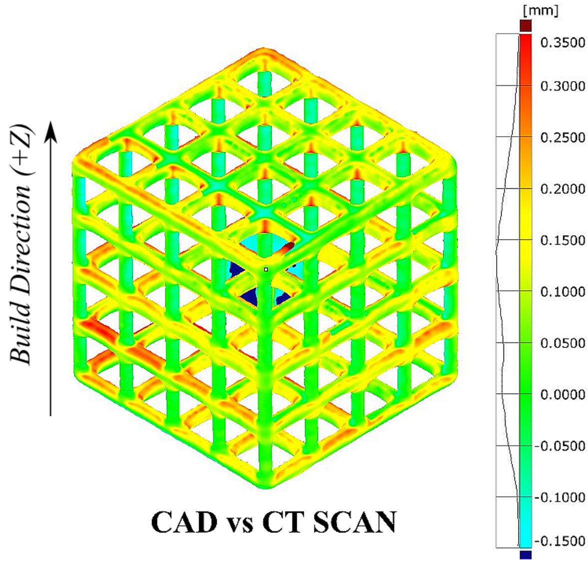

Figure 2. CAD and XCT scan surfaces comparison; Deviation (mm).

This comparison is informative; however, additional validation is needed to assess how node junctions deviate during the manufacturing process. In particular, node-level deviations should be quantified consistently, since local effects may not be fully captured by a global surface comparison.

3.2 Automated node finding and computation

The global alignment reduces the overall deviation between the designed geometry (CAD) and the manufactured part (XCT scan), but it does not enable a node-wise, local comparison of the two surfaces. Therefore, an automated procedure is required to identify and match corresponding nodes on the XCT geometry, so that local deviations can be quantified consistently.

After rigid CAD–XCT registration, the as-manufactured node locations are automatically recovered using the nominal CAD nodes as seeds. Fig. 3 summarizes the workflow: each designed node center c_i defines a Sphere of Interest (SOI) intended to enclose the local junction geometry (the node and the adjacent strut roots). The SOI provides a local search window, preventing ambiguity caused by the periodic repetition of lattice unit cells. The SOI radius r_{SOI} is chosen to fully capture node swelling while minimizing overlap with neighboring nodes. For every XCT surface vertex x we evaluate the signed distance function (SDF) of the SOI sphere $\varphi_{\mathrm{i}}(x)$. Vertices with $\varphi_{\mathrm{i}}(x) < 0$ lie inside the sphere and are kept; vertices with $\varphi_{\mathrm{i}}(x) \geq 0$ are discarded, Eq. 1. Then, the retained vertex subset for node i is V_i, Eq. 2.

$$\varphi_i(x) = \|x - c_i\| - r_{SOI} \qquad (1)$$

$$V_i = x_k \left(\varphi_i(x_k) < 0 \right) \qquad (2)$$

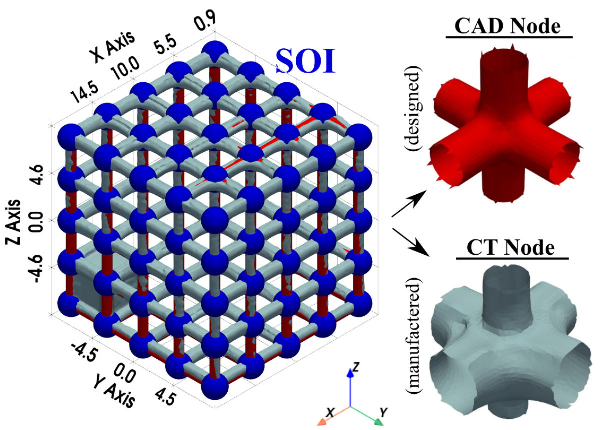

Figure 3. Node segmentation of XCT surfaces using Spheres of Interest (SOI) seeded from nominal CAD node centers.

This filtering step is computationally efficient because it only requires Euclidean distance evaluations and can be applied in a vectorized manner over all XCT vertices. The retained vertices define a local XCT surface patch around the node region. However, XCT meshes often exhibit non-uniform triangle sizes and vertex densities (for example, higher sampling in high-curvature areas), which can bias a simple mean or centroid estimate. For this reason, the extracted patch is uniformly remeshed to obtain a more even (approximately area-uniform) sampling of the surface, so that all parts of the node contribute more equally to the estimated center. After remeshing, the node location is estimated as a robust "center" of the patch; the geometric mean, described in Eq. 3, where N_v is the number of vertices inside the SOI.

$$p_i^{CT} = \frac{1}{Nv}\sum x_k \qquad (3)$$

In practice, for speed, we use the centroid of the uniformly remeshed vertices, which becomes the recovered XCT node center. Finally, the node deviation between ideal and manufactured is computed with Eq. 4. This provides per-node displacement components that can be plotted across the lattice to reveal spatial trends and identify outliers for deeper inspection. This algorithm has been developed in Python, including data analysis and visualization.

$$\Delta p_i = p_i^{CT} - c_i = [d_{x,i}, d_{y,i}, d_{z,i}]^T \qquad (4)$$

4. Experiments and results

This section presents the validation of the proposed workflow evaluated on an SLS strut lattice. After rigid CAD–XCT alignment, each CAD node seeds extraction of a XCT node patch, which is uniformly remeshed to recover XCT node centers. Node deviations are computed and visualized per node and across the node–edge graph to obtain a readable graph deviation field.

Table 1 summarizes the specimen and measurement settings. The lattice has external dimensions of 16 × 16 × 16 mm and a unit cell size of 4 × 4 × 4 mm, resulting in a regular array of repeated node–edge patterns. This controlled geometry is useful because it separates two effects: (i) deviations caused by registration or reconstruction noise and (ii) systematic manufacturing effects that vary with position (interior vs boundary) and height (bottom vs top, along the build direction +Z).

Fig. 4 reports node-level results. Fig. 4(a) plots d_x, d_y and d_z for all nodes (ordered by index), showing that displacement is not uniform and that peaks occur at specific node locations. This plot is informative because it separates directional effects: for example, a systematic bias in d_z would indicate build-direction drift, whereas larger variations in d_x or d_y can indicate lateral distortion or residual alignment error.

Table 1. *Specimen and XCT measurement summary*

Item	Value
Lattice type	Simple cubic strut-based lattice; node–edge graph representation
External dimensions	16 × 16 × 16 mm
Unit cell dimensions	4 × 4 × 4 mm
Strut diameter	1 mm
Manufacturing process	SLS, material: (PA12)
Build direction	+Z
XCT scanner / settings	Zeiss Metrotom 800/225 HR, 120 kV, 220 µA, Al 2.0 mm filter, exposure time 1000 ms, 1500 projections.
Voxel size / resolution	24.59 µm
Reconstruction/surface extraction	Adaptative local gradient

Fig. 4(b) shows a representative node (Node 50) with minimal deviation, where the manufactured node surface remains close to the designed CAD junction after alignment. Fig. 4(c) shows a node with maximal deviation (Node 120), where the XCT node surface visibly deviates from the designed junction shape. Importantly, the node-wise framework makes such outliers traceable: the node index identifies which junction to inspect in the XCT volume, while the deviation components provide a quantitative trigger for automated flagging.

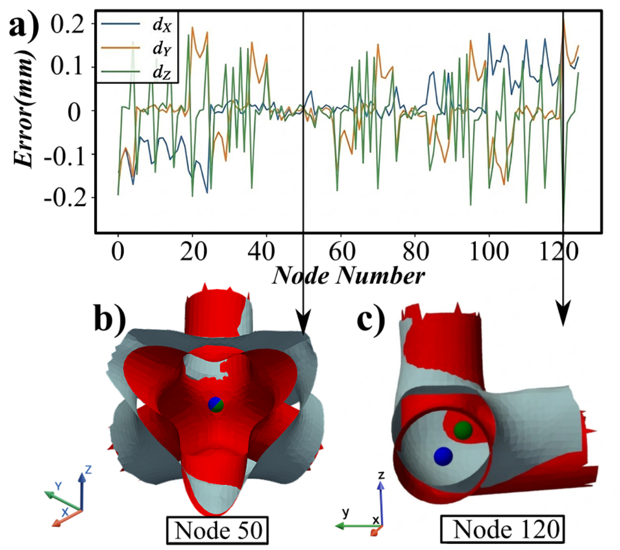

Figure 4. (a) Node difference between CAD and XCT scanned (Δp_i), designed vs manufactered. (b) Node 50 with minimal difference, and (c) Node 120 with maximum deviation.

Fig. 5 complements the node plots by visualizing deviations on the lattice graph. In Fig. 5(a) (isometric view), the deviation field highlights a spatial gradient from the interior (lower deviation) toward the boundary (higher deviation). The YZ view in Fig. 5(b) emphasizes height-dependent behavior along the build direction: lower planes near Z=-8 mm show reduced deviations compared with the upper planes near Z=+8 mm. Presenting results in graph form is helpful because it ties deviations directly to topology (nodes and their connections), which is the natural description used in downstream models such as homogenization or graph-based learning. Deviations are smaller near the lattice center and larger at the boundaries, likely because interior nodes have higher connectivity and are more constrained.

Deviations also increase with build height: nodes near the build plate show less deviation than those near the top, consistent with stronger support and heat sinking at lower layers and greater accumulated distortion above. Overall, these results demonstrate that the proposed segmentation provides a consistent CAD to XCT correspondence at the feature level and enables both local (node) and global (graph) deviation interpretation in a way that remains readable even for large lattices.

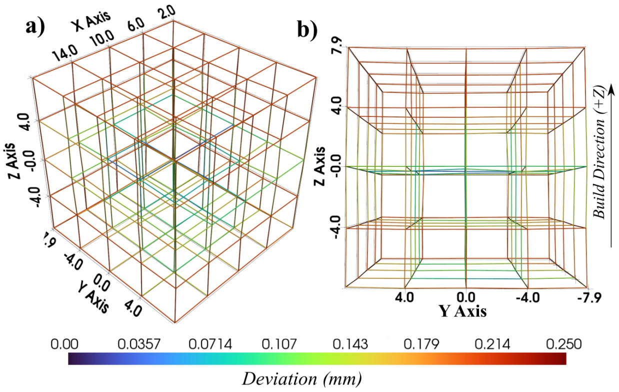

Figure 5. CAD-to-XCT Edge Deviation Field on the Lattice Graph. (a) Isometric view, and (b) YZ view.

5. Conclusions and future work.

An automated node-based workflow was used to compare a nominal CAD lattice with an as-manufactured XCT mesh. After rigid alignment, each CAD node was used as a seed to isolate a local XCT node region using a sphere-of-interest distance filter, and node centers were recovered from the filtered surface. Deviations are not uniform: they are typically smaller near the lattice core and larger near external boundaries, consistent with interior nodes being more constrained by higher connectivity while boundary nodes are more sensitive to free-surface process effects. The main effect is due to the best-fit allignement o the software. A build-direction trend is also observed: nodes closer to the build plate show lower deviations than nodes near the top.

The method enables repeatable node-by-node inspection and automated outlier detection. Future work will implement local best-fit alignment within each segmented zone, extend segmentation to strut-only regions for strut-level metrics, and link geometric deviations to mechanical response via simulation or homogenization with repeatability studies across builds and XCT settings.

Acknowledgments

This work was supported by grant PID2024-157236OB-I00 funded by MICIU/AEI/10.13039/501100011033 and, "ERDF A way of making Europe", by "ERDF/EU". The authors also thank the Gobierno de Aragón for its support within the framework of grants for research activity of recognized groups (T56_23R: GIFMA). Additionally, the authors acknowledge the use of Servicio General de Apoyo a la Investigación-SAI, Universidad de Zaragoza.

References

[1] F. Zanini, M. Sorgato, E. Savio, and S. Carmignato, "Dimensional verification of metal additively manufactured lattice structures by X-ray computed tomography: Use of a newly developed calibrated artefact to achieve metrological traceability," Additive Manufacturing, 2021. DOI 10.1016/j.addma.2021.102229

[2] F. Zanini, S. Carmignato, and E. Savio, "Two different experimental approaches for the uncertainty determination of X-ray computed tomography dimensional measurements on lattice structures," CIRP Journal of Manufacturing Science and Technology, 2024. DOI 10.1016/j.cirpj.2023.10.004

[3] A. du Plessis, A. Townsend, P. J. Scott, and R. K. Leach, "Dimensional metrology of additively manufactured lattice structures by combined tactile probe and X-ray tomography," Materials Design & Processing Communications, 2021. DOI 10.1002/mdp2.216

[4] D. Rathore, P. A. Williams, and K. S. Rao, "A Methodology for Computed Tomography-Based Non-Destructive Geometrical Evaluations of Lattice Structures by Holistic Strut Measurements Approach," Journal of Manufacturing Science and Engineering, 2021. DOI 10.1115/1.4049492

[5] B. Lozanovski, C. Downing, and A. T. Clare, "Non-destructive simulation of node defects in additively manufactured lattice structures," Additive Manufacturing, 2020. DOI 10.1016/j.addma.2020.101593

[6] B. Lozanovski, A. T. Clare, and R. S. Trask, "Image-Based Geometrical Characterization of Nodes in Additively Manufactured Lattice Structures," 3D Printing and Additive Manufacturing, 2021. DOI 10.1089/3dp.2020.0091

[7] L. Jiang, Y. Li, M. Dong, J. Zhao, and Y. Du, "Micro-CT-based strut shape analysis reveals manufacturing and post-processing effects in additively manufactured lattice structures," Additive Manufacturing Letters, 2025. DOI 10.1016/j.addlet.2025.100346

[8] J. E. Oosterbeek and J. R. Jeffers, "StrutSurf: A geometry and surface analysis tool for additively manufactured lattice structures," StrutSurf, 2022. DOI 10.1016/j.softx.2022.101043

[9] Q. Zheng, Y. Huang, H. Huang, L. Wang, L. Zhang, and S. Xu, "Quantitative surface characterisation and stress concentration factors of additively manufactured lattice struts," The International Journal of Advanced Manufacturing Technology, 2024. DOI 10.1007/s00170-024-13024-w

[10] L. Liu, B. Zhang, and B. Wang, "Dimensional effect and mechanical performance of additively manufactured lattice structures based on different node sizes," Virtual and Physical Prototyping, 2023. DOI 10.1080/17452759.2023.2240306

[11] H. Li, S. Huang, Y. Zhou, Z. Zhou, M. Gao, and C. Chen, "Effect of geometric defects on mechanical properties of lattice-filled thin-walled structures fabricated by additive manufacturing," Thin-Walled Structures, 2024. DOI 10.1016/j.tws.2024.112497

[12] D. Gallardo, L. C. Díaz-Pérez, J. A. Albajez, and J. A. Yagüe-Fabra, "Progress toward the Definition of Accuracy and Traceability of X-ray Computed Tomography Measurements for Polymer Additive Manufacturing," Polymers, 2024. DOI 10.3390/polym16101419

[13] M. Holgado, H. Villarraga-Gómez, M. Martínez, J. A. Yagüe-Fabra, and D. Gallardo, "Towards the Metrological Evaluation and Accuracy Improvement of Wall Thickness Estimations and Through-Hole Measurements in Industrial X-Ray Computed Tomography," Journal of Nondestructive Evaluation, 2025. DOI 10.1007/s10921-025-01269-8

[14] A. Chahid, L. M. Enquist, M. A. Gomaa, S. M. Wald, H. M. ElSawy, and N. M. Wereley, "Parametrically Designed Surface Topography on CAD Models of Additively Manufactured Lattice Structures for Improved Design Validation," Additive Manufacturing, 2021. DOI 10.1016/j.addma.2020.101731